Tikhonov-Type Regularization and the Finite Element Method Applied to Point Source Estimation in the Atmosphere

Roseane A.S. Albani* and Vinicius V.L. Albani†

February 26, 2019

Abstract

This work is concerned with the source identification problem in air pollution modeling. The forward problem is described by an advection-diffusion equation with physically realistic coefficients. It is solved by the combination of adaptive meshes and a stabilized finite element method. The source is estimated by Tikhonov-type regularization with a composite misfit function and an entropic penalty term. The composite misfit is given by the convex combination of ℓ_1 and ℓ_2 norms of the discrepancy between observed and predicted concentrations. Morozov's discrepancy principle is applied to simultaneously choose the regularization and the misfit combination parameters. Numerical experiments using Copenhagen field data is used to validate numerically the proposed methodology.

Keywords: Air Pollution Modeling, Stabilized Finite Elements Formulation, Source Identification, Tikhonov-type Regularization.

1 Introduction

The release of toxic materials to the atmospheric boundary layer (ABL) can bring serious consequences to those who will suffer its effects, like all kind of

*Dept of Mechanical Engineering, Federal University of Santa Catarina, Campus Trindade, 88.040-900 Florianopolis, Brazil, roseanealves75@gmail.com.br

†Dept of Mathematics, Federal University of Santa Catarina, , Campus Trindade, 88.040-900 Florianopolis, Brazil, v.albani@ufsc.br

vegetal and animal life. The leak of harmful gases may take place accidentally or deliberately in several ways, for example, leakage in gas pipelines, industrial accidental releases, or even terrorist attacks.

In such emergency situations, fast and accurate source estimation methodologies are of great significance to predict the source parameters (source strength and location) since they can be introduced in numerical forecast models to predict the transport and diffusion of the harmful contaminants into the atmosphere. Thus, improving the forecast of the source parameters allows the decision makers to look for better strategies regarding the evacuation and other protective measures in order to mitigate possible damages.

Since the identification of pollutant sources parameters is an intrinsic ill-posed problem, many different inverse problems techniques were proposed, some of them giving robust and reliable solutions. Such techniques can be divided into two main classes, namely, stochastic and deterministic methods.

The stochastic or Bayesian approach has been frequently using in source term estimation problems. See Wang et al. (2017) and references therein. In this class, the unknowns and the observed data are treated as random variables, which are related through the so-called likelihood function and the posterior probability distribution. Then, the reconstructions, which are given within confidence intervals, can be obtained by different sampling techniques, like point estimators or Monte Carlo Markov Chain methods. See for reference Somersalo and Kapio (2004). One of the main advantages of these methods is that they incorporate naturally the uncertainty in the observations and in the forward model. However, the sampling techniques can be computationally intensive, specially when the number of unknowns is large. This makes deterministic optimization techniques more attractive, since they are computationally cheaper and the reconstructions are robust. See Vogel (2002); Engl et al. (1996); Tarantola (2005).

In the deterministic or optimization class, a cost or objective function, which is usually based on the mean error between the measured and predicted concentrations, is given by different methods. See Wang et al. (2018) for different choices of cost functions. The desired parameters are, in general, global minimizers of the cost functional, which must be found by some optimization technique, like gradient-descent methods, genetic algorithm, simulated annealing, etc. See Long et al. (2010); Addepalli et al. (2011); Ma et al. (2014); Ma and Zhang (2016); Ma et al. (2017; 2018); Wang et al. (2018).

It is important to note that the precision of the source estimation will depend on the accuracy of both the measured data and the forward atmospheric dispersion model. In case of too noisy monitoring data or a poor prediction of the forward problem, the source estimation may greatly deviate from the real one.

Optimization methods coupled with the Gaussian plume model (GPM) have broadly been employed for the source parameter estimation, see Long et al. (2010); Addepalli et al. (2011); Ma et al. (2014); Ma and Zhang (2016); Ma et al. (2017; 2018); Wang et al. (2018). Using synthetic data, Long et al. (2010) combined the Genetic Algorithm with gradient descent techniques to determine the source parameters that fit the observed concentrations. They also estimated the minimum sensor requirements, given a particular configuration, needed to estimate the source term robustly. Addepalli et al. (2011) used a stochastic search to determine clever initial spatial parameters guess and Tikhonov-type regularization to identify the source. Ma et al. (2017) applied the Tikhonov regularization to identify the source strength and particle swarm optimization algorithm to estimate the source location. Wang et al. (2018) proposed the use of composite cost functions to identify the source location and source strength using Prairie-Grass field data. In this technique, two or more different cost functions are combined to define a composite objective function that appropriately balances sensitivity and robustness.

Concerning the forward problem, GPM has been widely applied to obtain the forward model solution in source estimation problems. However, the good reliance of such approaches is restricted to flat topography and stationary atmospheric conditions. To deal with the release of hazardous gases over an urban environment, or to include more physically relevant information about the ABL dynamics, for example, it is necessary to appeal for numerical solution methods. An improved Gaussian model was developed in Ma and Zhang (2016) in order to deplete the representative error from the analytical solution. Although this Gaussian solution had achieved better results in relation to the original forward problem formulation, its application to more complex scenarios seems to lack further investigation.

The ABL experiences a variety of regimes ranging from advection-to diffusion-dominated along the day. This fact imposes a challenging task to any solution method. The mathematical model for the forward problem is an advection-diffusion equation type. According to recurrently reported in the literature, the solution of advective-dominated problems faces several difficulties, as the appearance of nonphysical oscillations.

A numerical method to solve ABL dispersion models must be capable of dealing with such issues. Considering these points, we propose a combination of a finite element method (FEM) and adaptive mesh refinement to obtain the forward problem solution. This methodology considers the application of the stabilized finite element formulation proposed by Hughes et al. (1989) addressed to the solution of advective-diffusive equations. Finite element-based approaches have become an attractive option to the air pollution modeling

research field. See for example, Albani et al. (2015); Oliver et al. (2013); Monforte and Foguet (2014) and references therein.

The benefits of using finite elements based methods on air pollution modeling encompass the possibility of mesh adaptation to complex geometries and boundary conditions. In addition, it is possible to perform local refinements in those regions where the gradient solution changes abruptly such as near point source emissions along the downwind direction.

The forward model includes the time-evolving ABL structure by mean of parametric profiles for the wind speed and the vertical eddy-diffusivity, which, in turn, depend on the ABL stability regime. We assess the forward model by simulating a classical field experiment. The source parameters then, are subsequently obtained and evaluated with those data.

Since composite cost functions were successfully used for the source term estimation (Wang et al. (2018)) and in imaging problems (Yue et al. (2014); Yan (2013)), we propose an inversion technique based on Tikhonov-type regularization, where the data misfit or merit functional is given by the convex combination of the ℓ_2 and ℓ_1 norms of the discrepancy of measured and predicted concentrations. The penalty term is given by the Shannon entropy function. Another motivation to use a composite merit function is to treat differently uncertainty sources. In this case, we assume that the noise in the data is Gaussian, which justify the ℓ_2 misfit and the model uncertainty is treated as impulsive noise, leading to the ℓ_1-norm term. The regularization parameter and the parameters of the combination of ℓ_1 and ℓ_2 misfit terms are chosen accordingly to Morozov's discrepancy principle. See Morozov (1966).

For the best of our knowledge, the application of FEM to source estimation and the inversion technique aforementioned are new and constitute the main contribution of this paper.

This article is structured as follows: Section 2 is devoted to the forward problem formulation. In Section 3, the source identification problem and the estimation techniques are presented. The numerical experiments based on real data are the subject of Section 4. Concluding remarks are designed in Section 5.

2 Forward Problem

The goal of the present section is to introduce the so-called forward problem which consists of a partial differential equation (PDE) for the transport of a chemical species into the atmosphere, and its numerical solution based on FEM.

2.1 The Dispersion Model

The following mathematical model describes the dispersion of a single pollutant released from a point source in the atmospheric boundary layer. This model considers two transport mechanisms, that is advection in the horizontal direction (x, y-directions) and turbulent diffusion in the x, y, z-directions. The spatial domain for the computational model is the parallelepiped Ω in the ABL, which the dimensions will be specified later. The contaminant is released from a point source located at (x_s, y_s, z_s) within Ω during the time interval $[t_s - \varepsilon, t_s + \varepsilon]$, with $\varepsilon > 0$.

The problem of obtaining the mean pollutant concentration $C(x, y, z, t)$ at some spatial location $(x, y, z) \in \Omega$ and time $t \in [0, T]$ is given by solving the partial differential equation (PDE):

$$\frac{\partial C}{\partial t} + u\cos(\theta)\frac{\partial C}{\partial x} + u\sin(\theta)\frac{\partial C}{\partial y} - \frac{\partial}{\partial x}\left(K_x\frac{\partial C}{\partial x}\right) - \frac{\partial}{\partial y}\left(K_y\frac{\partial C}{\partial y}\right) - \frac{\partial}{\partial z}\left(K_z\frac{\partial C}{\partial z}\right) = Q\delta(x - x_s)\delta(y - y_s)\delta(z - z_s)\mathcal{X}_{[t_s-\varepsilon,t_s+\varepsilon]}(t), \quad (1)$$

where u is the wind velocity intensity and $\mathcal{X}_{[t_s-\varepsilon,t_s+\varepsilon]}(t)$ is the indicator function of the interval $[t_s - \varepsilon, t_s + \varepsilon]$, which is defined as

$$\mathcal{X}_{[t_s-\varepsilon,t_s+\varepsilon]}(t) = \begin{cases} 1, & \text{if } t \in [t_s - \varepsilon, t_s + \varepsilon], \\ 0, & \text{otherwise.} \end{cases}$$

We assume that the concentration field has no impact on the velocity field, which guarantees the linearity of the equation (1). The coefficients K_x, K_y and K_z represent the turbulent diffusion in the longitudinal, lateral and vertical directions respectively. The left-hand side terms of (1) account for the advection and diffusion of the pollutant, wherein the K-theory has been applied to model the turbulent fluxes. The right-hand side term accounts for the point source, where Q stands for the emission rate of the pollutant. Finally, θ is the wind direction angle.

2.2 The adjoint state

To find a minimizer for the Tikhonov-type functional, a gradient descent algorithm will be applied. To avoid solving two PDEs at each iteration during this procedure, we follow Pudykiewicz (1998), and replace the original PDE

problem by an adjoint one, which has to be solved only once, for each concentration measurement. This procedure furnishes a remarkable advantage when a computationally expensive solution method is applied to solve the dispersion model. More precisely, each observation $C^{obs}(x_j, y_j, z_j, T)$ is given by

$$C^{obs}(x_j, y_j, z_j, T) = \int_0^T \int_\Omega C(x, y, z, t) L_j(x, y, z, t) dx dy dz dt, \tag{2}$$

where $C(x, y, z, t)$ is the solution of the PDE problem (1), and L_j is the spatial filtering function for the sensor located at (x_j, y_j, z_j, t). See Yee et al. (2008). Since the operator that maps the emission source to concentration is linear, then, (2) is equivalent to

$$C^{obs}(x_j, y_j, z_j, T) = \int_\Omega C_j^*(x, y, z, t) S(x, y, z, t, x_s, y_s, z_s, t_s, Q) dx dy dz dt = \langle C_j^*, S \rangle, \tag{3}$$

where S denotes the emission source defined in (1) and C_j^* is the solution of the adjoint PDE

$$\frac{\partial C^*}{\partial t} - u\cos(\theta)\frac{\partial C^*}{\partial x} - u\sin(\theta)\frac{\partial C^*}{\partial y} - \frac{\partial}{\partial x}\left(K_x \frac{\partial C^*}{\partial x}\right) - \frac{\partial}{\partial y}\left(K_y \frac{\partial C^*}{\partial y}\right) - \frac{\partial}{\partial z}\left(K_z \frac{\partial C^*}{\partial z}\right) = L_j, \tag{4}$$

Equation (4) must be completed with initial and boundary conditions, given by

$$C^* = C_0 \quad \text{in} \quad \Omega \quad \text{for } t = 0, \tag{5}$$

$$\frac{\partial C^*}{\partial z} = 0 \quad \text{in} \quad z = z_0 \quad \text{and} \quad z = h \tag{6}$$

and

$$C^* = 0 \quad \text{elsewhere.} \tag{7}$$

The parameter h represents the boundary layer height which we define as the height of Ω. In addition, z_0 denotes the surface roughness length, which is also the height of the base of Ω. The PDE problem (4)-(7), associated with the coefficients u, K_x, K_y, K_z, the source strength Q and its location x_s, y_s, z_s, constitutes the forward problem formulation. Since the coefficients u, K_x, K_y, k_z

are functions of the solar radiation, they might change drastically depending on the meteorological conditions. Depending also on such meteorological conditions, the atmosphere can perform a diffusion or advection-dominated character.

Even when the atmosphere is diffusion-dominated, near the surface, the advection predominates and the equation possesses a hyperbolic character. That is an arduous task for any solution method. Hence, the employed solution methodology must be able to handle such issues.

It is well known that the classical Galerkin finite element method is not appropriate to deal with hyperbolic equations. Therefore, in this work, we use a stabilized FEM Galerkin/least-squares (GLS) designed to advective-diffusive equations. This is the subject of the next section.

2.3 Finite Element Formulation

We now shortly discuss the steps involved to obtain the finite element solution to the forward problem. The discretization process using a finite element method starts from a reformulation of the partial differential equation (4) jointly with its boundary conditions (5)-(7) as an equivalent variational problem. Concerning the problem (4), we aim to find the adjoint concentration C^* in the space φ of admissible functions such that

$$A(C^*, w) = 0 \quad \text{for all} \quad w \in W, \tag{8}$$

where A is a bilinear functional and W is a space of a special class of functions, as we shall see below. The bilinear functional $A(.,.)$ is given by

$$A(C^*, w) = \int_\Omega \left[w\frac{\partial C^*}{\partial t} - wu\cos(\theta)\frac{\partial C^*}{\partial x} - wu\sin(\theta)\frac{\partial C^*}{\partial y} + K_x\frac{\partial C^*}{\partial x}\frac{\partial w}{\partial x} + K_y\frac{\partial C^*}{\partial y}\frac{\partial w}{\partial y} + K_z\frac{\partial C^*}{\partial z}\frac{\partial w}{\partial z}\right] d\Omega, \tag{9}$$

In the context of the standard Galerkin method, φ usually denotes the trial space function and consists of all functions which are square integrable, have square integrable first derivatives over the computational domain Ω, and also satisfy the Dirichlet conditions. The space of functions W is similar to the trial space functions except that these functions are required to vanish on the Dirichlet portion of the boundary.

The sets φ and W are infinite-dimensional spaces of functions. So, in the context of FEM, φ and W are approximated by finite-dimensional subsets, denoted respectively by φ^h and W^h. These finite element spaces are

defined, among other things, according to a partition of the domain Ω into subdomains, called finite elements.

Hence, in the Galerkin method, the adjoint concentration C^* is approximated by the field $C^{*h} \in \varphi^h$, given by

$$C^{*h}(x, y, z, t) = \sum_{i=1}^{N} C_i^*(t)\phi_i(x, y, z), \tag{10}$$

where the unknowns $C_i^*(t) = C^{*h}(x_i, y_i, z_i, t)$ represent the concentration at the ith nodal point of the finite element mesh with coordinates (x_i, y_i, z_i), N is the dimension of the approximation spaces φ^h and W^h, and $\{\phi_1, \phi_2..., \phi_N\}$ is a particular orthonormal basis of both spaces φ^h and W^h.

In the standard Galerkin method, a semi-discrete system of equations for the unknown nodal functions C_i^* is obtained by substituting (10) in (8) and setting $w = \phi_i$ also in (8). As aforementioned, the standard Galerkin method gives rise to spurious oscillations when applied to advective-diffusive problems. Accordingly, we opt for the so-called Galerkin/Least Squares method (Hughes et al. (1989)), wherein the unknowns C_i^* are obtained by substituting (10) into an extended version of (8) given by

$$A(C^{*h}, w^h) + A_{GLS}(C^{*h}, w^h) = 0 \tag{11}$$

where

$$A_{GLS}(C^*, w) = \int_\Omega \tau \left(\frac{\partial C^*}{\partial t} + \Psi(C^*) \right) \Psi(w) d\Omega. \tag{12}$$

The operator $\Psi(.)$ is given by

$$\Psi(\zeta) = -u\cos(\theta)\frac{\partial \zeta}{\partial x} - u\sin(\theta)\frac{\partial \zeta}{\partial y} - \frac{\partial}{\partial x}\left(K_x \frac{\partial \zeta}{\partial x}\right) - \frac{\partial}{\partial y}\left(K_y \frac{\partial \zeta}{\partial y}\right) - \frac{\partial}{\partial z}\left(K_z \frac{\partial \zeta}{\partial z}\right) \tag{13}$$

The parameter τ is specified element-wise and determines the amount of numerical diffusion to be added in order to dump possible oscillations in the solution. Finding a closed form for τ is an open problem. If we set $\tau = 0$, the Galerkin formulation is retrieved. A review for this subject can be found in Volker and Knobloch (2007). For more details about the mathematical background of the present section see Ern and Guermond (2004); Donea and Huerta (2006). Furthermore, the reorganization of all of the terms of Equation (11) gives rise to the following semi-discrete system of equations:

$$\mathbf{F}(\mathbf{C}^*, \dot{\mathbf{C}}^*, t) = \mathbf{0} \tag{14}$$

wherein $\dot{\mathbf{C}}^*$ represents the time variation of the nodal concentration values and $\mathbf{C}^*$ indicates the nodal concentration values. To obtain $\dot{\mathbf{C}}^*$ values, a time discretization technique must be applied.

2.4 Turbulence Parameterization

Atmospheric transport and dispersion depend mainly on the wind intensity and direction, aside from the atmospheric turbulence state. The ABL structure changes along the day, and so, those quantities. To be capable of reproducing more realistic ABL conditions on the proposed dispersion model, parameterizations for u and K_z will be employed. Although u and K_z could be any function of the variables x, y, z and t, in this work, they will depend on (z, t) only. The dependence of these coefficients on t is implicitly given by the micro-meteorological parameters frictional velocity (u_*), Monin-Obukhov length (L) and the ABL height (h). Such parameterizations were taken from Ulke (2000) and they are presented below for the sake of completeness.

The vertical diffusion is given by:

$$K_z(z) = \kappa u_{*0} h \left(\frac{z}{h}\right)\left(1 - \frac{z}{h}\right)\left(1 + 6.9\frac{h}{L}\frac{z}{h}\right)^{-1} \tag{15}$$

for the stable condition ($h/L > 0$) and

$$K_z(z) = \kappa u_{*0} h \left(\frac{z}{h}\right)\left(1 - \frac{z}{h}\right)\left(1 - 22\frac{h}{L}\frac{z}{h}\right)^{1/4} \tag{16}$$

for the unstable condition ($h/L < 0$). The wind intensity is given by

$$u(z) = \frac{u_{*0}}{\kappa}\left\{\ln\frac{z}{z_0} - \left[1 - 6.9\frac{h}{L}\right]\left[\frac{z - z_0}{h} - \frac{6.9}{2}\frac{h}{L}\left[\frac{z^2 - z_0^2}{h^2}\right]\right]\right\} \tag{17}$$

for stable conditions and

$$u(z) = \frac{u_{*0}}{\kappa}\left\{\ln\frac{z}{z_0} + \ln\left[\frac{(1+\mu_0^2)(1+\mu_0)^2}{(1+\mu^2)(1+\mu)^2}\right] + 2(\arctan(\mu) - \arctan(\mu_0)) + \frac{2L}{33h}[\mu^3 - \mu_0^3]\right\} \tag{18}$$

for unstable conditions, with

$$\mu = \left(1 - 22\frac{h}{L}\frac{z}{h}\right)^{1/4} \quad \text{and} \quad \mu_0 = \left(1 - 22\frac{h}{L}\frac{z_0}{h}\right)^{1/4}.$$

3 The Identification Problem

The goal of the present section is to describe the estimation technique used in the numerical examples. We begin by introducing Tikhonov-type regularization. Then, the adaptation of this regularization technique to cope with different kinds of noise in the data is presented.

Firstly, let us assume that the concentration data is observed in all the finite element mesh points in the whole domain without noise or uncertainties. Denote this unrealistic set of measurements by $\tilde{C}$.

The *inverse problem* is then, the identification of the source location $(x^\dagger, y^\dagger, z^\dagger)$ and the source strength $Q^\dagger$, that satisfy the equation

$$\tilde{C} = C(x^\dagger, y^\dagger, z^\dagger, Q^\dagger), \tag{19}$$

where $C(x^\dagger, y^\dagger, z^\dagger, Q^\dagger)$ is the solution of the advection-diffusion PDE (1).

Unfortunately, only a scarce and noisy dataset C^{obs} is available, where C^{obs} and $\tilde{C}$ are related by

$$\|\tilde{C} - C^{obs}\|_{L^p} \leq \delta, \tag{20}$$

with $\delta > 0$ the noise level. Although the set of four unknowns is small, the corresponding least-square problem has more than one stationary point. See Addepalli et al. (2011). In addition, the dataset is highly noisy. Further, potential inaccuracies in the forward model makes the inverse problem of source estimation a difficult task that needs some regularization technique. See, for instance, the textbooks Engl et al. (1996), Scherzer et al. (2008), Vogel (2002) and Tarantola (2005) for more details.

Many different techniques can be applied to solve this inverse problem, but, Tikhonov-type regularization is probably the most widespread used method with successful results in many different applications. Its formulation is simple, in addition, it is well understood computationally and theoretically. See Engl et al. (1996); Scherzer et al. (2008); Tarantola (2005); Vogel (2002) and references therein. Hence, to solve the current inverse problem, we apply Tikhonov-type regularization as follows: find a set of parameters $(x_{min}, y_{min}, z_{min}, Q_{min})$ that minimizes the functional

$$\mathcal{F}(x, y, z, Q) = \phi(x, y, z, Q) + \alpha f(x, y, z, Q) \tag{21}$$

where

$$\phi(x,y,z,Q) = (1-\beta)\frac{\sum_{j=1}^{N_{sensors}}(C_j(x,y,z,Q)-C_j^{obs})^2}{\sum_{j=1}^{N_{sensors}}(C_j^{obs})^2} + \beta\frac{\sum_{j=1}^{N_{sensors}}|C_j(x,y,z,Q)-C_j^{obs}|^{1.001}}{\sum_{j=1}^{N_{sensors}}|C_j^{obs}|^{1.001}} \quad (22)$$

is the data misfit or merit function, $\alpha > 0$ is the regularization parameter, $\beta \in [0,1]$ is a free parameter and

$$f(x,y,z,Q) = x\log(x+2000) + y\log(y+5000) + z\log(z) + Q\log(Q), \quad (23)$$

is the regularizing functional. Note that, the misfit is a convex combination between the ℓ_2-norm and a smooth approximation of the ℓ_1 norm of the discrepancy between predicted and observed concentrations. The quantity C_j^{obs} is the experimental concentration for the jth sensor and $C_j(x,y,z,Q) = Q \cdot C_j^*(x,y,z)$ with $C_j^*(x,y,z)$ is the solution of the adjoint state (4).

The ℓ_2-norm in the misfit is related to a normally distributed noise in the data, whereas, the use of ℓ_1-norm is associated to impulsive noise, i.e., when there is a small number of mesh points where the noise is more prominent. See, e.g., Wohlberg and Rodriguez (2009), Zhang et al. (2014), and Darbon (2005) for some examples of the use of ℓ_1 misfit. To see the relation between ℓ_2 misfit and the Gaussian noise, see Kaipio and Somersalo (2006).

The choice of the norm in the misfit depends on the typical distribution of the noise source in experimental data of the problem under consideration. There are many different choices, not restricted to ℓ_1 and ℓ_2 norms, for the merit function, for example, it is also possible to choose ℓ_p norm with $p > 0$, ℓ_∞ norm, Kullback-Leibler divergence or the Poisson log-likelihood functional. See Wen et al. (2017), Clason (2012), Resmerita and Anderssen (2007) and the textbooks Tarantola (2005) and Vogel (2002). In Addepalli et al. (2011), the authors proposed a misfit function in the source identification problem that compensates the difference of magnitudes in the measured data. It is also possible to combine different misfits, as above, whenever different kinds of noise are present in the data. See, e.g., Yue et al. (2014), Yan (2013) and Wang et al. (2018).

Some misfit functions are non-differentiable, like the ones based on ℓ_1, ℓ_∞ and ℓ_p, with $0 < p < 1$, norms. So, sometimes it is useful to approximate such merit functions by some smooth ones. For example, as we did above, the ℓ_1-norm can be replaced by some ℓ_p-norm with $p > 1$ but close to 1. See, for example, Attoucha and Cominettib (1999) and Wen et al. (2017). The differentiability of the merit function and of the penalty f is important

since it allows the use of gradient-based techniques in the minimization of the Tikhonov-type functional (21). For example, quasi-Newton, conjugated gradient and steepest descent methods can be used to solve the corresponding optimization problem. See Vogel (2002). For more details on optimization techniques, see Nocedal and Wright (2006).

Other combinations of functionals in the misfit could be tested, however, in recent works, this one has proved to be useful for imaging processing problems where the presence of more than one source of noise is detected. See, e.g., Yue et al. (2014), Yan (2013) and Langer (2017). It is also important to mention that ℓ_1-based and, principally, ℓ_2-based merit functions are the most common choices in a plethora of applications, presenting reliable results. See Tarantola (2005), Vogel (2002) and Kaipio and Somersalo (2006) and references therein.

Another important feature of Tikhonov-type regularization is the choice of the regularizing term. We use the Shannon entropy, since maximum entropy is considered as a universal method to find the most reasonable distribution in the presence of incomplete data, see Skilling (1988) and Shore and Johnson (1980). Since, this is the case in the problem under consideration, this is a natural choice. In addition, entropy functional is extensively used in inverse problems, specially when the ℓ_1-norm is the norm of the parameters set. See, Eggermont (1993), Amato and Hughes (1991) and Resmerita and Anderssen (2007).

The parameters β, and α are free and we chose them based on Morozov's discrepancy principle. See Morozov (1966). There are other choice rules, see, for example, Vogel (2002) and Langer (2017), but, this particular one is widespread used successfully.

4 Results and Discussion

This section is devoted to the numerical validation of the techniques used to solve both, the forward and the inverse problems. This is performed by using the experimental data sets from the Copenhagen field campaign (Gryning (1981)).

4.1 Forward Problem Validation

The Copenhagen field experiment was conducted under neutral and unstable atmospheric conditions. The tracer sulfur hexafluoride (SF_6) was released without buoyancy from a tower at a height of 115m, and after, collected 2-3m above ground level at locations up to three crosswind arcs of tracer sampling

units, positioned radially 2, 4 and 6Km from the point of release. The site was mainly residential having a roughness length of 0.6m. Three successive 20 min averaged tracer concentrations (runs 1,2 and 3) were measured, resulting in a total sampling time of 1 hour. For this work, we choose about 20 sampling points of SF_6 concentration from "run 1" and "run 2" and then, we averaged these values to evaluate the numerical solution and subsequently, to estimate the source parameters. Meteorological data measured during the field campaign as well as a complete description from the Copenhagen experiments can be found in Gryning (1981); Gryning and Lyck (1984; 2002).

We employed concentration and micrometeorological data from October 19, 1978 given by $h = 1120$[m], $u_* = 0.39$[m/s] and $L = -108$[m]. The average wind direction during the sampling period was $\theta = 290^o$. The longitudinal and lateral eddy diffusivity coefficients values $K_x = K_y = 50$ [m^2/s] are usually applied during unstable conditions [Arya (2001), p. 272].

Figure 1 shows a schematic representation of the sampling units during the experiments. The x-axis points towards East direction and y-axis, towards the North. The base of the computational domain can also be seen in Fig.1. Hence, the computational domain dimensions are $\Omega = [-2, 8] \times [-5, 5] \times [0, h]$ [Km].

We made use of non-uniform adaptive finite element meshes. This procedure performs grid refinements only when it is necessary, that is, along the wind direction near the source of emission, where the concentration gradients are steepest. The initial mesh is locally refined around the source and then, an iterative procedure generates the mesh according to an error estimation depending on the the concentration gradient. The computational domain was divided into tetrahedral elements.

During the sampling period the meteorological conditions presented no changes, as well as the measured concentrations. Hence, stationary conditions are considered and time derivative is set to zero in Equation (14).

The numerical solution for the adjoint state problem (4), was obtained for a total of 20 sampling points. Therefore, we performed a total of 20 simulations of the forward problem. The computational domain has a parallelepiped form with a volume of 112 [km^3], divided in about 3.500.000 tetrahedron linear elements. Of course the number of mesh elements depends on the sensor location, however, they don't diverge that much.

This numerical procedure was developed and solved by using COMSOL Multiphysics 4.4 (COMSOL, Burlington, USA). The computational time spent to simulate each run of the forward problem ranged from 3-8 minutes (depending on the sensor position). We ran all the experiments on a Core i5 3.2GHz computer with 16GB of RAM memory under Windows 7 professional 64-bits.

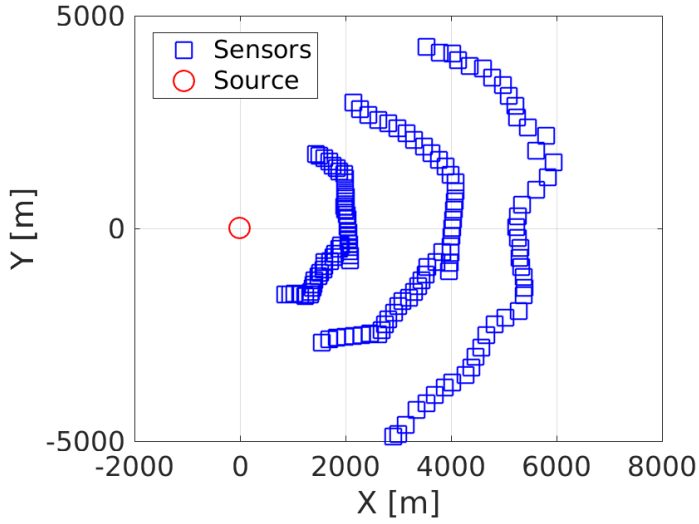

Figure 1: Schematic representation for the sampling units and source position during the Copenhagen Experiment.

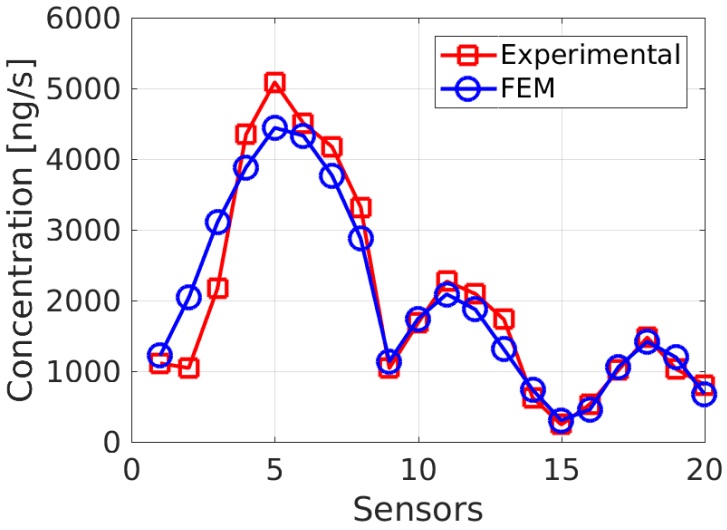

Figure 2: Comparison between experimental and simulated data corresponding to the Copenhagen data.

Figure 2 presents a comparison of FEM solution and experimental concentration data. The FEM solution is adherent to the observed concentrations.

To access the agreement between observed (O) and predicted (P) concentrations the statistical indices proposed by Hanna (1989) were employed.

The indices are defined as follows.

Normalized Mean Square Error: $\text{NMSE} = \dfrac{\overline{(C_0 - C_p)}^2}{\overline{C_0}\overline{C_p}}$,

Correlation Coefficient: $R = \dfrac{\overline{(C_0 - \overline{C_0})(C_p - \overline{C_p})}}{\sigma_0 \sigma_p}$,

Fractional Bias: $FB = \dfrac{\overline{C_0} - \overline{C_p}}{0.5(\overline{C_0} + \overline{C_p})}$,

Fractional Standard Deviations: $FS = \dfrac{(\sigma_0 - \sigma_p)}{0.5(\sigma_0 + \sigma_p)}$,

Factor of two : $FAC2 = 0.5 \leq \dfrac{C_p}{C_0} \leq 2.$

Solution	NMSE	R	FB	FS	FAC2
Ideal values	0	1	0	0	1
Present work	0.03	0.92	0.02	0.12	1

Table 1: Statistical indices for the Finite Element solution for the dispersion model based on the Copenhagen field experiment data.

The bars in the indices above denote the mean values of the quantities. The Correlation Coefficient shows a high degree of relationship between experimental and numerical concentrations. The positive and small values of FB indicates that the observed concentrations are lightly underestimated by the finite element solution presented in this work. Finally, FAC2 value shows that 100% of the numerical concentrations are between the half and double of the experimental concentration. The excellent agreement between the calculated and the measured concentrations give us the confidence to estimate the source parameters from those results.

4.2 Determination of the Source Location and Strength

The goal of the present section is to illustrate that the Tikhonov-type regularization technique presented in Section 3 is able to provide accurate solutions to the source estimation inverse problem. For all the numerical experiments provided here, we consider the same experimental dataset used in Section 4.1.

Concerning the choice of the parameters α and β in the Tikhonov-type functional (21), we tested the values

$$\beta = j \cdot 0.05, \text{ with } j = 0, 1, ..., 20,$$

and

$$\alpha = 10^{-x}, \text{ with } x = 5, 6, 7.$$

The values of α and β that we consider acceptable are those which the ℓ_2 normalized discrepancy

$$\sqrt{\frac{\sum_{j=1}^{N_{sensors}}(C_j(x,y,z,Q)-C_j^{obs})^2}{\sum_{j=1}^{N_{sensors}}(C_j^{obs})^2}},$$

is bellow 0.15. This choice was inspired by Morozov's discrepancy principle (Morozov (1966)) and the value 0.15 is based on the ℓ_2 discrepancy obtained with the true values for the source position and the source strength. Of course, in real applications, this value is in general not available, but it can be estimated based on the sensors, on the meteorological conditions in the field and on the numerical method chosen to solve the direct problem.

As aforementioned, the number of sensors was set at $N_{sensors} = 20$. We compare the reconstructed parameters obtained when the forward problem is solved by FEM with the one provided by GPM. It is important to remark that GPM is the simplest atmospheric dispersion model available. It is an analytical solution to the advection-diffusion equation with constants coefficients. A description of GPM can be found, for instance, in Seinfeld and Pandis (2006). In this set of numerical experiments, the GPM solution was obtained for the atmospheric stability Pasquill class C (slightly unstable), which corresponds to the experimental case employed in the previous section. We have used the same GPM solution presented in Addepalli et al. (2011).

To initialize the minimization of the Tikhonov-type functional (21), we choose the initial source position (x_0, y_0, z_0) and the initial source strength Q_0 at random. In other words, x_0, y_0, z_0 and Q_0 are draws of the uniform random variables:

$$x_0 \sim U[-2000, 8000],\ y_0 \sim U[-5000, 5000],$$
$$z_0 \sim U[0.6, 1120],\ \text{and}\ Q_0 \sim U[0, 20],$$

where $U[a, b]$ denotes the uniform random distribution in the interval $[a, b]$.

The reconstructed values of the source position and the source strength using FEM for different values of the parameters β and α can be found in Tables 2, 4 and 6. Tables 3, 5 and 7 present the parameters reconstructed using GPM. Only the values that satisfy the discrepancy, i.e., the ℓ_2-misfit is below 0.15, are included in the tables.

For $\alpha = 10^{-5}$ there are already values of β that satisfy the discrepancy using both methods, FEM and GPM. However, we present the results using different values of α to illustrate that, as α decreases, the accuracy of the reconstructed parameters using GPM increases a bit.

β	x	y	z	Q	ℓ_2-Misfit	ℓ_1-Misfit
0.70	46.53	10.31	118.97	3.38	0.127	0.100
0.75	-110.35	89.46	108.63	3.42	0.137	0.105
0.80	69.48	-0.44	116.94	3.31	0.127	0.100
0.85	-35.54	45.78	112.27	3.37	0.135	0.104
0.90	-90.16	78.06	109.03	3.41	0.136	0.105
0.95	-110.23	89.38	108.65	3.42	0.137	0.105
1.00	404.70	-160.91	125.45	3.13	0.110	0.100
True	0	0	115	3.20		

Table 2: Reconstructed position and source strength of the source emission using FEM. The values of $\beta \in [0, 1]$ correspond to ℓ_2-misfit values below 0.15. The true values are also present for comparison. The regularization parameter is set at $\alpha = 10^{-5}$.

β	x	y	z	Q	ℓ_2-Misfit	ℓ_1-Misfit
0.85	-1157.55	577.93	105.60	6.04	0.136	0.107
0.90	-1157.55	577.93	105.60	6.04	0.136	0.107
0.95	-1157.54	577.93	105.60	6.04	0.136	0.107
1.00	-1104.17	547.92	107.42	5.92	0.136	0.106
True	0	0	115	3.20		

Table 3: Reconstructed position and source strength of the source emission using GPM. The values of $\beta \in [0, 1]$ correspond to ℓ_2-misfit values below 0.15. The true values are also present for comparison. The regularization parameter is set at $\alpha = 10^{-6}$.

The tables also show that, for smaller values of the ℓ_2-misfit, the reconstructions are less accurate. This is in accordance with the rule of thumb of inverse problems, that says we cannot overfit the data.

The most accurate reconstructions for each value of α, using both FEM and GPM, can be found in Table 8. By the comparison between the best results for each α, we can observe that, the reconstructions obtained with FEM are much more accurate than those provided by GPM, whenever the same technique to solve the inverse problem is applied. This fact illustrates that with more accurate solutions of the forward problem the results for the inverse problem can be indeed improved.

Furthermore, for almost all values of α, our best results are with β different from 0 and 1. $\beta = 0$ and $\beta = 1$ correspond to Tikhonov-type functionals with single ℓ_2-misfit and single ℓ_1-misfit, respectively. This is also an evidence that it is worth to use composite misfit functionals to solve the inverse

β	x	y	z	Q	ℓ_2-Misfit	ℓ_1-Misfit
0	479.29	-196.06	126.43	3.07	0.109	0.101
0.05	515.74	-213.04	127.99	3.06	0.108	0.101
0.10	451.72	-182.58	126.41	3.09	0.109	0.101
0.15	83.52	-3.32	121.14	3.36	0.126	0.100
0.20	463.38	-188.18	125.35	3.06	0.109	0.101
0.30	406.70	-157.44	124.91	3.10	0.110	0.100
0.35	324.35	-121.32	127.04	3.22	0.112	0.100
0.40	113.71	-18.81	119.53	3.30	0.123	0.100
0.45	165.75	-45.47	118.37	3.24	0.120	0.099
0.50	275.34	-95.54	122.98	3.22	0.114	0.100
0.55	24.93	24.10	119.74	3.42	0.128	0.102
0.60	48.82	12.05	117.28	3.34	0.127	0.100
0.65	169.76	-44.63	124.73	3.33	0.120	0.099
0.70	-25.39	46.73	114.72	3.40	0.133	0.103
0.80	-76.55	73.01	110.72	3.41	0.135	0.105
0.85	114.25	-18.71	120.25	3.31	0.123	0.100
0.90	327.10	-124.59	129.06	3.24	0.113	0.100
True	0	0	115	3.20		

Table 4: Reconstructed position and source strength of the source emission using FEM. The values of $\beta \in [0, 1]$ correspond to ℓ_2-misfit values below 0.15. The true values are also present for comparison. The regularization parameter is set at $\alpha = 10^{-6}$.

problem, as highlighted by Wang et al. (2018). One possible reason for this is the fact that the data can be corrupted by more than one noise source with different probability distributions.

The minimization of the Tikhonov-type functional (21) was performed by the function LSQNONLIN from the optimization toolbox of MATLAB, with the settings below:

- Maximum number of function evaluations: 35000.
- Maximum number of iterations: 25000.
- Termination tolerance on the objective function value: 10^{-25}.
- Termination tolerance on the current point: 10^{-25}.

Each minimization took approximately 60 seconds in an Intel Core i7-4510U CPU @ 2.00GHz laptop with 8GB RAM running MATLAB R2017a in Ubuntu Linux 16.04.05 LTS.

β	x	y	z	Q	ℓ_2-Misfit	ℓ_1-Misfit
0.05	-953.27	489.13	0.6	5.26	0.127	0.125
0.10	-994.99	505.41	0.6	5.36	0.129	0.121
0.15	-1045.51	525.46	0.6	5.49	0.132	0.116
0.20	-1059.52	528.56	0.6	5.50	0.135	0.113
0.25	-1046.94	520.11	0.6	5.45	0.136	0.112
0.30	-1075.84	532.83	0.6	5.53	0.138	0.111
0.35	-1071.38	530.44	0.6	5.52	0.138	0.111
0.40	-1066.16	527.66	0.6	5.52	0.138	0.111
0.45	-1059.01	523.85	0.6	5.51	0.138	0.111
0.50	-1053.33	520.82	0.6	5.50	0.138	0.111
0.55	-1050.23	519.16	0.6	5.49	0.138	0.111
0.60	-1028.55	507.61	0.6	5.46	0.139	0.110
0.65	-762.76	394.73	195.41	5.96	0.112	0.098
0.70	-986.93	485.42	0.6	5.40	0.141	0.110
0.75	-953.27	467.49	0.6	5.36	0.144	0.110
0.80	-1060.76	524.78	0.6	5.51	0.138	0.111
0.85	-945.00	463.08	0.6	5.35	0.145	0.109
0.90	-919.33	475.69	201.87	6.24	0.124	0.098
0.95	-944.75	462.95	0.6	5.35	0.145	0.110
1.00	-972.53	477.72	0.6	5.39	0.142	0.110
True	0	0	115	3.20		

Table 5: Reconstructed position and source strength of the source emission using GPM. The values of $\beta \in [0, 1]$ correspond to ℓ_2-misfit values below 0.15. The true values are also present for comparison. The regularization parameter is set at $\alpha = 10^{-6}$.

Hence, based on the results above and the comparisons between solutions obtained with FEM and GPM, we can conclude that, the combination of more accurate solutions of the forward problem with the use of composite misfit functions in Tikhonov-type regularization is indeed worth to provide precise reconstructions of the source strength and the source position.

5 Concluding Remarks

Based on the premise that more accurate modeling of the forward problem potentially improves the solution of the inverse problem, we proposed a stabilized FEM formulation to numerically solve the atmospheric dispersion model. This methodology allowed the introduction of physically relevant

β	x	y	z	Q	ℓ_2-Misfit	ℓ_1-Misfit
0	409.99	-160.55	126.38	3.14	0.109	0.101
0.05	415.21	-165.14	127.02	3.13	0.109	0.100
0.10	264.73	-90.23	126.32	3.27	0.115	0.100
0.25	479.24	-195.92	127.75	3.08	0.109	0.101
0.30	212.52	-66.23	122.90	3.27	0.117	0.100
0.40	25.65	24.66	117.93	3.38	0.128	0.101
0.50	48.31	12.95	118.12	3.35	0.127	0.100
0.55	367.34	-139.93	122.83	3.13	0.110	0.100
0.60	273.40	-96.44	130.22	3.29	0.116	0.100
0.70	234.30	-75.06	123.70	3.25	0.117	0.100
0.75	-22.91	47.08	116.67	3.43	0.132	0.103
True	0	0	115	3.20		

Table 6: Reconstructed position and source strength of the source emission using FEM. The values of $\beta \in [0, 1]$ correspond to ℓ_2-misfit values below 0.15. The true values are also present for comparison. The regularization parameter is set at $\alpha = 10^{-7}$.

characteristics of the ABL. Although such techniques are not completely new, for the best of our knowledge, this was not yet applied to source estimation problems. In general, the forward problem is solved by GPM, which has limited applications in more realistic situations.

In addition, FEM formulation can be used jointly with wind profiles given by the solution of the Navier-Stokes equations, whenever the hypotheses made in this work are not valid, for example, when dealing with non-homogeneous boundary layers.

Numerical tests illustrated that the predicted concentrations given by FEM solution were quite close to the observed data. This was corroborated by means of statistical indices, usually employed to evaluate the dispersion models.

To address more appropriately the uncertainty sources in the data and in the forward problem solution, we solved the inverse problem by Tikhonov-type regularization, where the misfit functional was given by the convex combination of the ℓ_2 and the ℓ_1 norms of the discrepancy between predicted and observed concentrations. The regularizing or penalty term was the Shannon entropy, which is commonly used in applications. The regularization parameter and the parameter that controls the weight of each norm in the misfit function were chosen accordingly to the Morozov's discrepancy principle. This particular combination of inverse problems techniques was also a contribution of this article.

β	x	y	z	Q	ℓ_2-Misfit	ℓ_1-Misfit
0	-547.79	289.23	201.49	5.62	0.107	0.0989
0.05	-549.63	289.73	202.07	5.64	0.107	0.099
0.10	-551.56	290.21	202.60	5.65	0.107	0.099
0.15	-553.91	290.88	203.15	5.66	0.107	0.099
0.20	-556.15	291.37	203.88	5.67	0.107	0.099
0.25	-560.47	293.09	204.27	5.68	0.107	0.099
0.30	-568.37	296.67	204.44	5.70	0.108	0.099
0.35	-565.33	294.07	205.94	5.71	0.108	0.098
0.40	-571.10	296.67	206.00	5.73	0.108	0.098
0.45	-582.17	302.02	205.66	5.74	0.108	0.098
0.50	-590.59	306.07	205.39	5.76	0.108	0.098
0.55	-604.14	312.64	205.05	5.78	0.108	0.098
0.60	-609.34	315.21	205.09	5.79	0.108	0.098
0.65	-614.26	317.75	205.44	5.80	0.108	0.098
0.70	-619.97	320.70	205.88	5.81	0.109	0.098
0.75	-629.01	325.36	206.55	5.82	0.109	0.098
0.80	-645.53	333.89	207.77	5.86	0.109	0.098
0.85	-660.13	341.44	208.85	5.89	0.110	0.098
1.00	-794.80	411.19	204.88	6.06	0.116	0.098
True	0	0	115	3.20		

Table 7: Reconstructed position and source strength of the source emission using GPM. The values of $\beta \in [0, 1]$ correspond to ℓ_2-misfit values below 0.15. The true values are also present for comparison. The regularization parameter is set at $\alpha = 10^{-7}$.

Table	Method	α	β	x	y	z	Q
Table 2	FEM	10^{-5}	0.70	46.53	10.31	118.97	3.38
Table 3	GPM	10^{-5}	1.00	-1104.17	547.92	107.42	5.92
Table 4	FEM	10^{-6}	0.55	24.93	24.10	119.74	3.42
Table 5	GPM	10^{-6}	0.65	-762.76	394.73	195.41	5.96
Table 6	FEM	10^{-7}	0.40	25.65	24.66	117.93	3.38
Table 7	GPM	10^{-7}	0	-547.79	289.23	201.49	5.62
-	True	-	-	0	0	115	3.20

Table 8: Comparison of the best reconstructions obtained using FEM and GPM for each value of α.

Numerical tests using Copenhagen experimental field campaign showed that the proposed technique provided solutions considerably precise.

The computational cost of the inverse problem solution was comparable with typical solutions in the literature. Concerning the forward problem, the computational cost to run all the simulations at the same time (all sensors) might be considerably reduced by a parallelization procedure.

Therefore, the proposed methodology has a strong appeal to be used during real leakage events.

References

B. Addepalli, K. Sikorski, E. Pardyjak, and M. Zhdanov. Source characterization of atmospheric releases using stochastic search and regularized gradient optimization. *Inverse Problems in Science and Engineering*, 19 (8):1097–1124, 2011.

R. Albani, F. P. Duda, and L. Pimentel. On the modeling of atmospheric pollutant dispersion during a diurnal cycle: A finite element study. *Atmospheric Environment*, 118:19–27, 2015.

U. Amato and W. Hughes. Maximum entropy regularization of Fredholm integral equations of the first kind. *Inverse problems*, 7(6):793–808, 1991. doi: 10.1088/0266-5611/7/6/004.

S. P. Arya. *Introduction to Micrometeorology*. Academic Press, 2001.

H. Attoucha and R. Cominettib. L^p approximation of variational problems in L^1 and L^∞. *Nonlinear Analysis: Theory, Methods & Applications*, 36 (3):373–399, 1999. doi: 10.1016/S0362-546X(98)00078-9.

C. Clason. L^∞ fitting for inverse problems with uniform noise. *Inverse Problems*, 28(10):104007, 2012.

J. Darbon. Total variation minimization with L^1 data fidelity as a contrast invariant filter. In *Proceedings of the 4th international symposium on image and signal processing and analysis (ISPA 2005)*, pages 221–226. Citeseer, 2005.

J. Donea and A. Huerta. *Finite Element Method for Flow Problems*. Wiley, 2006.

P. Eggermont. Maximum Entropy Regularization for Fredholm Integral Equations of the first kind. *SIAM J. Math. Anal.*, 24:1557–1576, 1993. doi: 10.1137/0524088.

H. Engl, M. Hanke, and A. Neubauer. *Regularization of Inverse Problems*, volume 375 of *Mathematics and its Applications*. Kluwer Academic Publishers Group, Dordrecht, 1996.

A. Ern and J. L. Guermond. *Theory and Practice of Finite Elements*. Springer, 2004.

S. E. Gryning. Elevated source sf_6 - tracer dispersion experiments in the Copenhagen area. Technical report, Riso-R-446, Riso nacional laboratory, 187 pp, 1981.

S. E. Gryning and E. Lyck. Atmospheric dispersion from elevated sources in urban area: Comparison between tracer and experiments and the model calculations. *J. Climate Appl. Meteor.*, 23:651–660, 1984.

S. E. Gryning and E. Lyck. The copenhagen tracer experiments: Reporting of measurements. Technical Report 1054, Technical University from Denmark, Denmark. Forskningscenter Risoe, 2002.

S. R. Hanna. Confidence limit for air quality models as estimated by bootstrap and jacknife resampling methods. *Atmos. Environ.*, 23:1385–1395, 1989.

T. Hughes, L. Franca, and G. Hulbert. A new finite element formulation for computational fluid dynamics: Viii. the galerkin/least-square method for advective-diffusive equations. *Comput. Method. in Appl. M.*, 73:173–189, 1989.

J. Kaipio and E. Somersalo. *Statistical and computational inverse problems*, volume 160. Springer Science & Business Media, 2006.

A. Langer. Automated parameter selection in the $L^1 - L^2$-TV model for removing Gaussian plus impulse noise. *Inverse Problems*, 33(7):074002, 2017. doi: 10.1088/1361-6420/33/7/074002.

J. Long, S. Haupt, and G. Young. Assessing sensitivity of source term estimation. *Atmospheric Environment*, 44:1558–1567, 2010.

D. Ma and Z. Zhang. Contaminant dispersion prediction and source estimation with integrated gaussian-machine learning network model for point source emission in atmosphere. *Journal of Hazardous Materials*, 311:237–245, 2016.

D. Ma, S. Wang, and Z. Zhang. Hybrid algorithm of minimum relative entropy-particle swarm optimization with adjustment parameters for gas source term identification in atmosphere. *Atmospheric Environment*, 94: 637–646, 2014.

D. Ma, W. Tan, Z. Zhang, and J. Hu. Parameter identification for continuous point emission source based on tikhonov regularization method coupled with particle swarm optimization algorithm. *Journal of Hazardous Materials*, 325:239–250, 2017.

D. Ma, W. Tan, Q. Wang, Z. Zhang, J. Gao, X. Wang, and F. Xia. Location of contaminant emission source in atmosphere based on optimal correlated matching of concentration distribution. *Process Safety and Environmental Protection*, 117:498–510, 2018.

L. Monforte and A. P. Foguet. A multimesh adaptive scheme for air quality modeling with the finite element method. *International Journal for Numerical Methods in Fluids*, 74:387–405, 2014.

V. Morozov. On the solution of functional equations by the method of regularization. *Dokl. Math.*, 7:414–417, 1966.

J. Nocedal and S. Wright. *Numerical Optimization*. Springer Series in Operations Research and Financial Engineering. Springer, 2006.

A. Oliver, G. Montero, R. Montenegro, E. Rodríguez, E. J.M., and A. Pérez-Foguet. Adaptive finite element simulation of stack pollutant emissions over complex terrains. *Energy*, 49:47–60, 2013.

J. Pudykiewicz. Application of adjoint tracer transport equations for evaluating source parameters. *Atmospheric environment*, 32(17):3039–3050, 1998. doi: 10.1016/S1352-2310(97)00480-9.

E. Resmerita and R. Anderssen. Joint Additive Kullback-Leibler Residual Minimization and Regularization for Linear Inverse Problems. *Math. Method Appl. Sci.*, 30:1527–1544, 2007. doi: 10.1002/mma.855.

O. Scherzer, M. Grasmair, H. Grossauer, M. Haltmeier, and F. Lenzen. *Variational Methods in Imaging*, volume 167 of *Applied Mathematical Sciences*. Springer, New York, 2008.

J. H. Seinfeld and S. N. Pandis. *Atmosphric Chemistry and Physics: From Air Pollution to Climate Change*. Wiley-Interscience, 2006.

J. Shore and R. Johnson. Axiomatic derivation of the principle of maximum entropy and the principle of minimum cross-entropy. *IEEE Transactions on information theory*, 26(1):26–37, 1980. doi: 10.1109/TIT.1980.1056144.

J. Skilling. The axioms of maximum entropy. In *Maximum-Entropy and Bayesian Methods in Science and Engineering*, pages 173–187. Springer, 1988.

E. Somersalo and J. Kapio. *Statistical and Computational Inverse Problems*, volume 160 of *Applied Mathematical Sciences*. Springer, 2004.

A. Tarantola. *Inverse problem theory and methods for model parameter estimation*, volume 89. SIAM, 2005.

A. G. Ulke. New turbulent parameterization for a dispersion model in the atmospheric boundary layer. *Atmos. Environ.*, 34:1029–1042, 2000.

C. Vogel. *Computational methods for inverse problems*, volume 23. SIAM, 2002.

J. Volker and P. Knobloch. On spurious oscillations at layers diminishing (sold) methods for convection diffusion equations: Part i: A review. *Comput. Method. in Appl. M.*, 196:2197–2215, 2007.

Y. Wang, H. Huang, L. Huang, and B. Ristic. Evaluation of bayesian source estimation methods with prairie grass observations and gaussian plume model: A comparison of likelihood functions and distance measures. *Atmospheric Environment*, 152:519–530, 2017.

Y. Wang, H. Huang, L. Huang, and X. Zhang. Source term estimation of hazardous material releases using hybrid genetic algorithm with composite cost functions. *Engineering Applications of Artificial Intelligence*, 75:102–113, 2018.

F. Wen, P. Liu, Y. Liu, R. Qiu, and W. Yu. Robust Sparse Recovery in Impulsive Noise via ℓ_p-ℓ_1 Optimization. *IEEE Transactions on Signal Processing*, 65(1):105–118, 2017. doi: 10.1109/TSP.2016.2598316.

B. Wohlberg and P. Rodriguez. An ℓ_1-TV algorithm for deconvolution with salt and pepper noise. In *Acoustics, Speech and Signal Processing, 2009. ICASSP 2009. IEEE International Conference on*, pages 1257–1260. IEEE, 2009. doi: 10.1109/ICASSP.2009.4959819.

M. Yan. Restoration of images corrupted by impulse noise and mixed Gaussian impulse noise using blind inpainting. *SIAM Journal on Imaging Sciences*, 6(3):1227–1245, 2013. doi: 10.1137/12087178X.

E. Yee, F.-S. Lien, A. Keats, and R. D'Amours. Bayesian inversion of concentration data: Source reconstruction in the adjoint representation of atmospheric diffusion. *Journal of Wind Engineering and Industrial Aerodynamics*, 96(10-11):1805–1816, 2008. doi: 10.1016/j.jweia.2008.02.024.

L. Yue, H. Shen, Q. Yuan, and L. Zhang. A locally adaptive l^1-l^2 norm for multi-frame super-resolution of images with mixed noise and outliers. *Signal Processing*, 105:156–174, 2014. doi: 10.1016/j.sigpro.2014.04.031.

F. Zhang, R. Dai, and H. Liu. Seismic inversion based on l^1-norm misfit function and total variation regularization. *Journal of Applied Geophysics*, 109:111–118, 2014. doi: doi.org/10.1016/j.jappgeo.2014.07.024.